Journal of
Composites Science

MDPI

Article

Animal Biopolymer-Plant Biomass Composites: Synergism and Improved Sorption Efficiency

Mohamed H. Mohamed, Inimfon A. Udoetok and Lee D. Wilson *

Department of Chemistry, University of Saskatchewan, 110 Science Place, Saskatoon, SK S7N 5C9, Canada; mom133@mail.usask.ca (M.H.M.); inu850@mail.usask.ca (I.A.U.)

* Correspondence: lee.wilson@usask.ca; Tel.: +1-306-966-2961; Fax: +1-306-966-4730

Received: 22 December 2019; Accepted: 27 January 2020; Published: 1 February 2020

Abstract: Pelletized biomaterial composites that contain chitosan (C) and torrefied wheat straw (S) at variable weight composition (C:S) were prepared using a facile blending process. The fractional content of the wheat straw was studied to elucidate the role of biomass on the pelletized product and effects of S-content on the physicochemical properties relevant to adsorption phenomena. Chitosan pellets (with and without S) were characterized by spectroscopic (FT-IR and ^{13}C NMR) and thermal (TGA and DSC) techniques to provide support for their respective C:S composition. Confocal microscopy using fluorescein (FL) as a dye probe revealed the presence and an increase in the accessibility of the active sites for the composite pellets according to the S-content (wt %). Equilibrium and kinetic sorption studies using FL and reactive black (RB) dyes revealed an incremental adsorption affinity of the pellets with anionic dyes in variable charge states (FL and RB). The trend for dye adsorption parallels the incremental S-content (wt %) in the composite pellets. This study reports a *first-example* of a low-cost, facile, and sustainable approach for the valorization of straw and chitosan suitable for sorption-based applications in aqueous media.

Keywords: chitosan; straw; lignins; sorption; pelletization; biomass; biocomposite; valorization

1. Introduction

Biomass refers to matter usually derived from plants and animal byproducts or waste [1]. The production of biomass is steadily increasing due to increased agricultural production, where under-utilized biomass waste is a concern from a sustainable management and resource recovery perspective [2]. Major components of biomass often derived from plants or animals include polysaccharides and lignins, where straw and chitosan are common biomaterials derived from plant and animal sources, respectively. Wheat straw is a multicomponent biomass that contains cellulose, hemicellulose, and lignins; whereas chitosan is a single component polysaccharide comprised of β-(1→4)-2-amino-2-deoxy-D-glucopyranose units [3,4]. Studies have shown that valorization of straw [5] often requires energy intensive conversion to yield fuels, along with chemical modification strategies for enhanced utilization as an adsorbent [6,7]. Chitosan is a chitin-based material that has utility as an adsorbent for the controlled removal of diverse chemical species from water [8].

The utilization of pristine biomass such as wheat straw and chitosan as effective adsorbent materials is often limited by a low or negligible adsorption capacity due to limited physicochemical properties such as surface area, solubility, porosity, and ineffective phase separation from water following adsorption processes in aqueous media. For example, chitosan is soluble at acidic conditions and cannot be used in its pristine form for solid-liquid adsorption processes in aqueous acidic media [9]. Similarly, wheat straw has been reported to exhibit little or no affinity for the adsorption of anionic dyes due to its negative surface charge at ambient pH [10]. Chemical modification strategies such as cross-linking, grafting, and bead formation have been employed to improve the adsorption properties

and insolubility of such biomass. These strategies address the insolubility of chitosan in acidic media along with an improvement of the adsorption properties of the biomass. However, the utility of chitosan as a low cost and efficient adsorbent requires further optimization. For example, Mahaninia and Wilson reported improved adsorption of phosphate anions from aqueous solution upon bead formation and/or cross-linking of chitosan but reiterated that the technique was limited by the kinetics of adsorbate diffusion into the bead microstructure [11]. As well, Kim et al. reported the low uptake of reactive black (RB) dye using similar bead systems [12]. Bertolino et al. reported that chitosan-based nanocomposites possess excellent thermal properties [13] for packaging, tissue engineering, and pharmaceutical applications [14], whereas Lissuzo et al. reported on the utility of chitosan-based nanocomposites for drug delivery [15]. In the case of wheat straw biomass, Romar-Gasalla et al. reported a low uptake of anion species due to its negative surface charge, whereas others report the effectiveness of modified wheat straw for the adsorption of cationic adsorbates [7].

The adsorption properties of chitosan-straw composites prepared via physical blending with chitosan are inferred to vary for anionic adsorbates upon the use of torrefied wheat straw. Torrefaction of wheat straw results in the reduction of its cellulosic composition; thereby increasing its hydrophobic nature and textural porosity [16,17]. The biomass composite materials reported herein via co-pelletization with chitosan in aqueous acetic acid are anticipated to display enhanced adsorption properties due to enhancement of textural properties. This strategy is hypothesized to afford a positive surface charge for the pelletized composite and greater porosity by the introduction of voids or defects that afford greater adsorbate diffusion, in contrast to more dense chitosan bead systems obtained by the phase-inversion synthesis. Component blending and pelletization are envisaged to afford adsorbent materials with improved phase separation over powdered materials that favour scalability for solid phase extraction (SPE) processes in aqueous media. Previous studies have reported the utility of blending binary systems in their powdered form with further chemical modification, [18] and co-pelletization of torrefied wheat straw with peanut shells [19]. To the best of our knowledge, this study reports a *first-example* that demonstrates the utility of co-pelletization between chitosan and wheat straw at variable straw content, along with characterization of the adsorption properties of these composites with anionic dyes. This study contributes to the field of biocomposites in several aspects: i) New insight on the role of variable straw content on the physicochemical properties of co-pelletized chitosan, ii) new insight on the effect of variable straw content on the affinity of co-pelletized chitosan for anionic dyes, and iii) new insight on the effect of variable straw content on the adsorption kinetics of anionic dyes by co-pelletized chitosan.

2. Materials and Methods

2.1. Materials

Low molecular weight chitosan (50,000–190,000 Da) industrial grade with ~75%–85% deacetylation, (C) was obtained from the POS Pilot Plants Corp (Project 2300). Glacial acetic acid (AcA), hydrochloric acid (HCl), and 8-dram vials (screw thread with polyvinyl-faced pulp lined closure) were obtained from Fisher Scientific (Mississauga, ON, Canada). Torrefied straw (S) at 280 °C was obtained after treatment of locally sourced wheat straw in the torrefaction facility at the University of Saskatchewan in the College of Engineering. Fluorescein (FL) and reactive black V (RB) dyes were obtained from Sigma-Aldrich (Oakville, ON, Canada) and all materials were of the highest grade and purity and used as received unless specified otherwise.

2.2. Methods

2.2.1. Pellet Preparation

Chitosan was pelletized by doping with acetic acid (0.1 M) using an extrusion method to make a pelletized biopolymer (CP). Composite pellets were produced using a similar method by adding S to C

at various contents (wt %): 10% chitosan-straw (CS-10), 30% (CS-30), and 50% (CS-50). The range of S content was determined by assessing the upper limit (ca. 50 wt %) of the mechanical stability of the composites in aqueous media, whereas the lower limit (ca. 10 wt %) was established by the onset of notable thermal effects in the thermal stability profiles for straw (results not shown). The intermediate region (ca. 30%) between these limits was guided by a midpoint in composition (ca. 30 wt %) between the lower and upper bound limits. The pellets were air-dried after the extrusion step and then stored in sealed vials for further characterization, as outlined below.

2.2.2. Pellet Characterization

FTIR Spectroscopy

A Bio-RAD FTS-40 IR spectrophotometer was used to characterize the functional groups present in the chitosan pellet (CP), pristine straw (S), and the composite co-pellets (CS-10, CS-30, and CS-50). The crushed pellets in powder form were analysed without dilution using KBr in reflectance mode. The DRIFT (Diffuse Reflectance Infrared Fourier Transform) spectra were obtained with a spectral resolution of 4 cm^{-1}, where 512 scans were recorded over the 400–4000 cm^{-1} spectral range at 295 K.

Thermal Gravimetric Analysis (TGA)

The thermal stability of the precursors (chitosan pellet (CP) and pristine straw (S)) and the composite pellets (CS3-10, CS3-30, and CS3-50) were evaluated with a Q50 TGA system (TA Instruments, New Castle, DE, USA), where N_2 was used as the carrier gas (balance flow: 10.00 mL/min and sample flow: 90.00 mL/min) and the heating rate was set to 5 °C min^{-1} to an upper limit of 500 °C.

Differential Scanning Calorimetry (DSC) Studies

A TA Q20 thermal analyzer was used to elucidate the DSC profiles of CP, pristine straw, and the composite materials. The scan rate was set to 5 °C min^{-1}, where dry N_2 gas (flow rate: 50 mL/min) was used for temperature regulation and sample compartment purging. The samples (ca. 5 mg) were hermetically sealed in aluminum pans and analyzed by heating from 50 to 180 °C. The results were reported as a plot of heat flow (W/g) versus temperature (°C).

^{13}C Solid State NMR Spectroscopy

The ^{13}C solids NMR spectra of the powdered materials were acquired using a Bruker AVANCE III HD spectrometer equipped with a 4 mm DOTY CP-MAS (cross polarization with magic angle spinning) solids probe operating at 125.77 MHz (^1H NMR frequency = 500.23 MHz). The ^{13}C CP-MAS spectra were acquired using a spinning speed of 10 kHz, ^1H-90 pulse of 3.5 μs, contact time of 0.75 ms, and a ramp pulse on the ^1H channel. Then, 4000 scans were accumulated with a recycle delay of 2 s, where all spectra were recorded using a 71 kHz SPINAL-64 decoupling sequence during acquisition and adamantane was the external standard (δ = 38.48 ppm for the low field signal).

Confocal Laser Scanning Microscopy (CLSM)

Confocal laser scanning microscopy (CLSM; Leica SP5) images were acquired after equilibrating the pelletized samples in 10 mL of a 20 μM fluorescein (FL) solution for 24 h. A thin slice of each stained pellet was used for the CLSM measurements. Images were taken using the 488 nm excitation line of an Argon laser with the 500–650 nm emission range and a step size of 3 um. All images were collected using the same settings (z-stacks = 102 um). The acquired digital images were further analyzed using ImageJ software, version 1.52 s.

2.2.3. Sorption studies

Equilibrium Sorption Studies

The equilibrium adsorption properties of the pellets were evaluated using fluorescein (FL) and reactive black (RB) dyes, respectively. An equimolar FL and RB solution (ca. 302 μM) were respectively prepared at ambient pH and 30 mL of each dye solution was added to the 10 mL vials that contained the pelletized samples (ca. 100–130 mg). A horizontal shaker table was used for the sample equilibration for 24 h at 295 K, where the dye adsorption capacity of the pellets with the respective dyes was determined, as previously described [20].

Kinetic Sorption Studies

Changes in the physicochemical properties of the pellets was further probed by elucidating their adsorption profiles using in situ kinetic studies. A 33 μM solution of RB and 21 μM solution of FL was used herein. One pellet (ca. 100 mg) was added to a 4.5 mL cuvette followed by the addition of 3 mL of dye solution. The cuvette with the pellet immersed in the dye solution was immediately transferred to a double beam spectrophotometer (Varian CARY 100) at 295 ± 0.5 K, where the adsorption of the dye by the pellets was monitored temporally for 24 h. The kinetic profiles were plotted as the quantity of the dye removed at variable time (Q_t) vs. time (t).

3. Results and Discussion

3.1. FT-IR

The IR spectra of the pristine CP and S, along with the composite pellets (CS3-10, CS3-30, and CS3-50) are shown in Figure 1. The results reveal that the IR bands of CP are less apparent with incremental S-content in the composite pellets. The bands for CP include C–O–H, C–O–C, and C–N–H asymmetric stretching at 1171 cm^{-1}, [21] where a vibrational band ascribed to adsorbed acetic acid onto CP occurs at 1668 cm^{-1}. The spectra of the co-pellets show spectral overlap and broadening of the bands at 1668 cm^{-1} from CP and 1710 cm^{-1}, where the latter band concurs with aldehydes and ketones reported for torrefied straw [22]. The composites reveal an attenuation of the 1171 cm^{-1} band with increasing S-content, in agreement with composite formation between C and S. Evidence of composite formation between C and S include the broadening and shift of the band at 1710 cm^{-1} due to possible associative interactions between acetic acid and the aldehydes/ketones present in S. The acid-base forms of acetic acid can act as both hydrogen bond donor and acceptor groups [23].

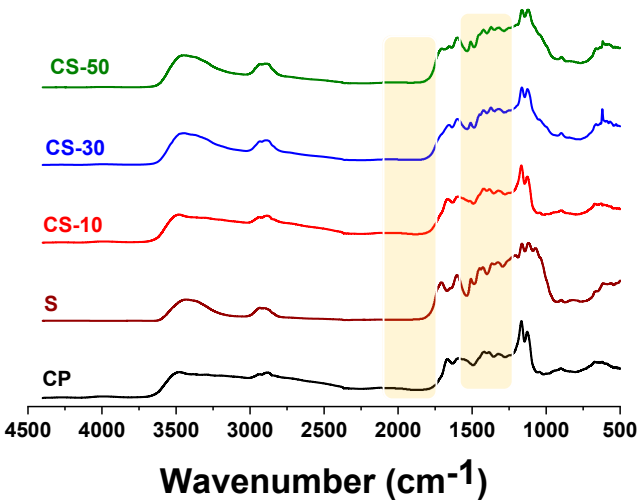

Figure 1. FT-IR spectra for chitosan pellet (CP), pristine straw (S), chitosan-straw (CS-10, CS-30, and CS-50) composite samples at variable composition.

3.2. ^{13}C Solid State NMR Spectroscopy

Figure 2 shows the ^{13}C solids NMR spectra of the pristine materials (CP and S) and the composite pellets (CS-10, CS-30, and CS-50). The CP spectral signatures for C1-C6 (cf. Figure 6 in [20]) are attenuated as more S incorporates into the composite pellets. The ^{13}C signatures for S include those from hemicellulose (40–120 ppm) and lignins (120–190 ppm) [22]. While the hemicellulose signatures are overlapped with those from CP, the lignin signatures ca. 141–160 ppm appear in the composite pellets when the S-content was increased. The NMR and IR results provide complementary support that composite formation occurs at variable C:S content.

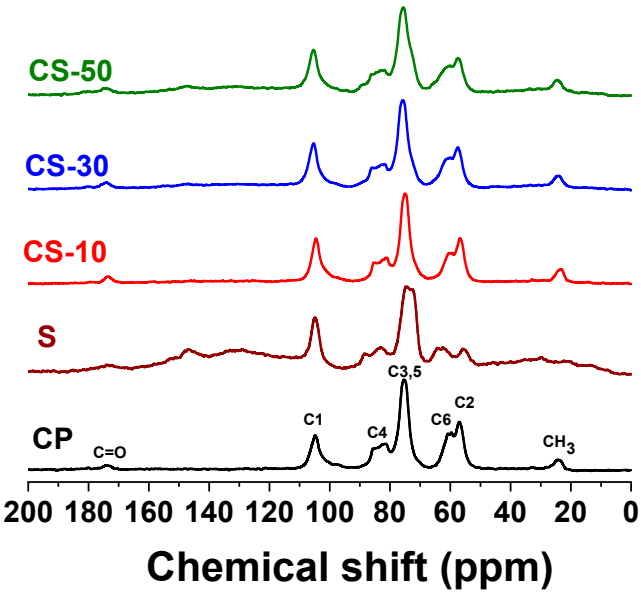

Figure 2. ^{13}C solid state NMR for CP, S, CS-10, CS-30, and CS-50.

3.3. Thermal Analysis

Figure 3a,b show weight loss and derivative plots from the TGA profiles of S, CP, and the composite pellets (CS-10, CS-30, and CS-50). The first thermal event (30–150 °C) was attributed to the loss of water and acetic acid. Although S is hydrophobic, the CP and CS materials contain acetic acid where reduced water loss occurs for increasing S-content in the composites: CP > CS-10 > CS-30 > CS-50. The CP and S both exhibit another single thermal event with maximum decomposition temperature ($T_{max;}$ cf. Table 1) at 298 and 338 °C, respectively. On the other hand, the composite pellets display thermal events related to both chitosan and straw near 298 and 345 °C, respectively. Each respective thermal event for the composite materials vary according to the weight ratio of CP and S. The T_{max} for chitosan in the CS materials increases by ca. 1 °C while that for straw differs by ca. 4 °C. This technique also provides complementary evidence of composite formation for the pellets. This approach offers a method that provides semi-quantitative support of the composition of the CS materials.

The DSC results (cf. Figure 4) provide further evidence of the role of bound water and acetic acid, as shown from the TGA results. The T_{max} and transition enthalpy values are attenuated in the CS pellets relative to CP except for CS-10 (91.4, 200, 237, 127, and 119 J/g for S, CP, CS-10, CS-30, and CS-50, respectively). Since CP contains acetic acid, the decrease in the enthalpy value with a greater straw content in the composite pellets provides further support on the hydrophobic nature of S that does not support greater hydration of the pellets. This results in a lower energy required to break the interaction of both bound water in the pellets with high S-content. The variation in the T_{max} values do not follow a clear trend according to the relative sample composition.

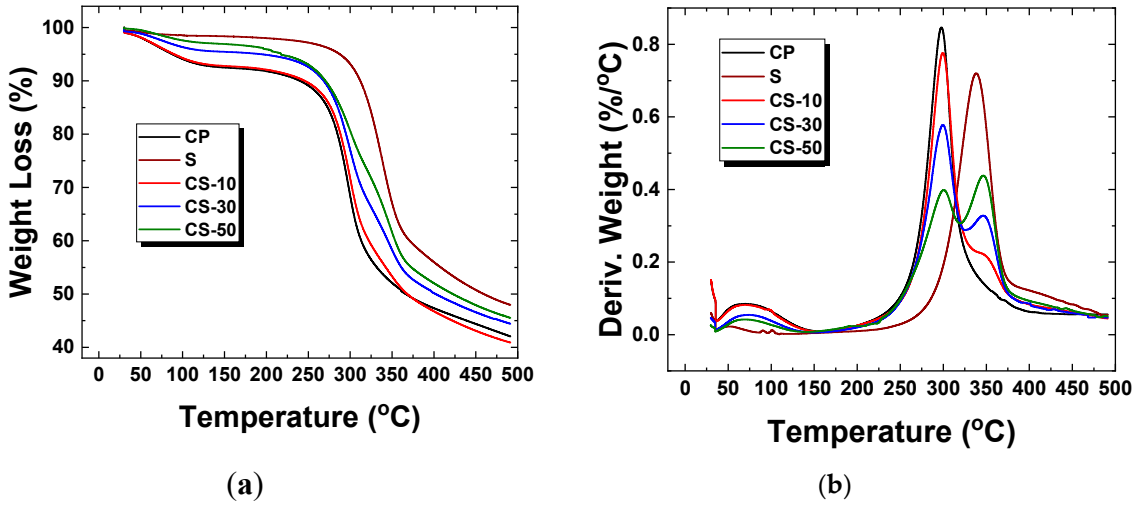

Figure 3. (**a**) Weight loss (%) and (**b**) differential thermal analysis (DTA) plots (weight loss/°C vs. temperature) derived from thermal gravimetric analysis (TGA) for CP, S, CS-10, CS-30, and CS-50 samples.

Table 1. Thermal properties from thermal gravimetric analysis (TGA) and differential scanning calorimetry (DSC) for the materials.

Material	TGA	DSC	
	T_{max} (°C)	$\Delta_{trs}H$ (J/g)	T_{max} (°C)
CP	70.6 ± 0.4, 298 ± 1.5	200 ± 6.0	104 ± 0.3
S	48.1 ± 0.2, 338 ± 1.7	91.4 ± 2.7	85.0 ± 0.3
CS-10	70.5 ± 0.4, 299 ± 1.5, 347 ± 1.7	237 ± 7.1	93.3 ± 0.3
CS-30	71.7 ± 0.4, 300 ± 1.5, 346 ± 1.7	127 ± 3.4	84.5 ± 0.3
CS-50	70.4 ± 0.4, 300 ± 1.5, 346 ± 1.7	119 ± 3.6	94.6 ± 0.3

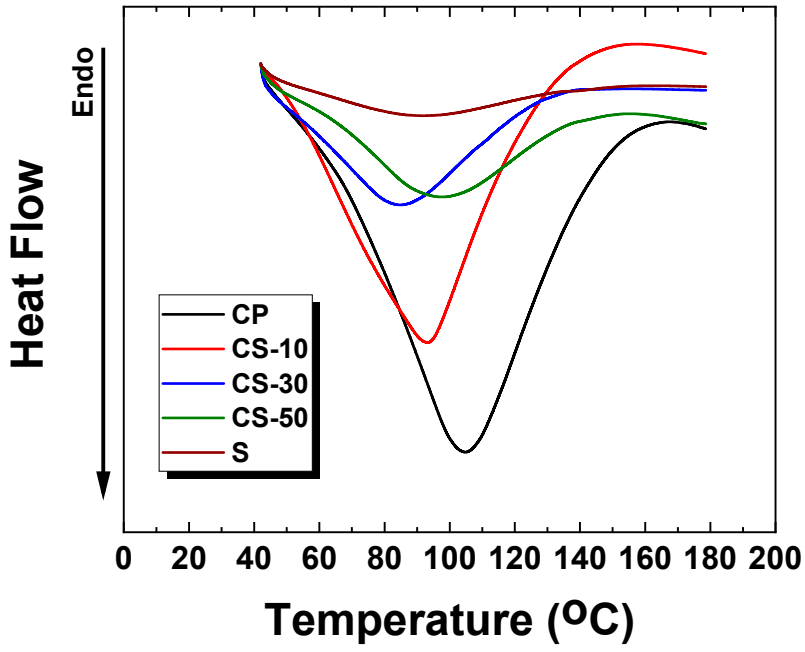

Figure 4. Differential scanning calorimetry (DSC) for CP, S, CS-10, CS-30, and CS-50 samples.

3.4. Confocal Laser Scanning Microscopy (CLSM)

CLSM is a common technique used to examine the surface properties of materials using either light emission or absorption techniques [24]. Herein, a fluorescein dye probe [25,26] was used to map the surface of the pellets. In the native form, S is not stained by the dye, whereas CP is readily stained. In Figure 5, the CLSM images are shown for CP and the composite pellets. The intensity of dye is attenuated with greater incorporation of S into the CP biomaterial. The incorporation of straw biomass results in improved access to the active adsorption sites of chitosan via the creation of voids or defects in the pellets upon composite formation for the pelletized material.

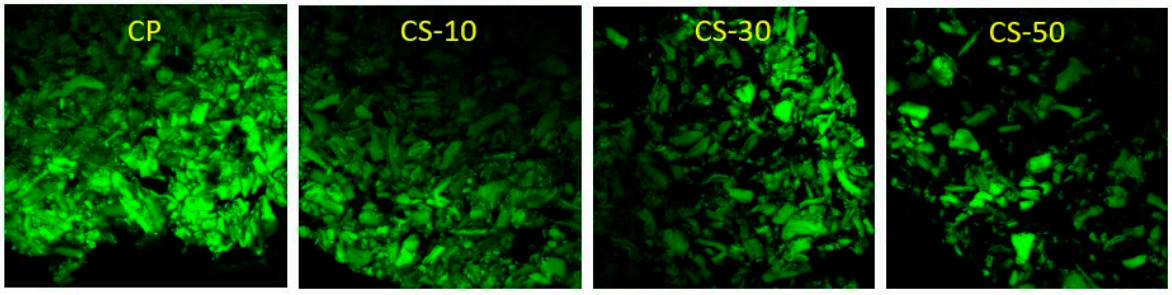

Figure 5. Confocal imaging for CP, S, CS-10, CS-30, and CS-50 after equilibration with fluorescein.

3.5. Sorption Studies

In order to gain insight on the physicochemical properties of the modified pellets for sorption-based applications, dye probes with variable charge state (fluorescein (FL) and reactive black (RB)) were studied. An in situ kinetic and batch equilibrium sorption studies were employed using FL and RB. These anionic dye probes were chosen due to various criteria: *i*) High molar absorptivity to detect small changes in the microenvironment, *ii*) variable hydrophile-lipophile character to provide insight on the sorption mechanism, and *iii*) the use of ambient conditions since pH adjustment was not required to conduct the sorption analysis. Figure 6a reveals the sorption capacity (Q_e; μmol/g) at equilibrium, where various experimental parameters were held constant throughout (adsorbent weight, dye concentration, and contact time). The results obtained reveal that the presence of S as a single component additive has negligible uptake affinity for FL and RB. In the case of CP and the CS materials, FL has greater sorption capacity relative to RB by ca. 25-fold, where the sorption capacity of the composite pellets is greater as the S-content increased. The difference in uptake between FL and RB may relate to the size difference of the dyes, where RB is approximately twice that of FL in terms of their relative molecular volume (RB; 674 $Å^3$ and FL; 311 $Å^3$) and surface area (RB; 740 $Å^2$ and FL; 315 $Å^2$). Moreover, RB has a greater dipole moment (D; Debye) relative to FL (RB; 20.8 D and FL; 7.41 D). The aforementioned properties were estimated using Spartan '18 V1.1.0 from Hartree–Fock SCF calculations that were performed using an equilibrium geometry for water in the ground state. The basis set used was 6-31G (*). The difference in these properties favor more efficient diffusion of FL into the pellets over the RB dye. The variation in dye diffusion kinetics finds support as noted by parallel differences in the dye sorption capacity of the composite pellets. The kinetic uptake (*cf.* Figure 6b) for CP and CS pellets indicate that a moderate diffusion rate occurs during the first 30 min, whereas the presence of S in the composite pellets attenuate diffusion effects for the slow process. It was inferred that the presence of S within the composite enhanced the intraparticle dye diffusion within the pellet microstructure due to the presence of voids or defects. The enhancement of the internal surface area of the pellet accounts for the greater access between the dyes and the active sites of chitosan that result in greater sorptive uptake. To provide further support, CP was imbibed in water for 24 h (hereafter denoted as CP-S) prior to obtaining kinetic adsorption isotherms for each dye system. The isotherm results (*cf.* Figure 6b) reveal a two-fold increase in the sorption capacity of CP-S relative to CP, along with a reduction in the slow diffusion phase of the sorption process. To further

probe the effects of dye molecular size on the adsorption properties of the CS-50 pellets, in situ kinetics were performed using FL and RB dyes. Figure 6c illustrates the in situ kinetic profiles of RB and FL at μM levels. In order to keep the absorbance in aqueous solution of both dyes near unity, variable dye concentration (33 μM for RB and 21 μM for FL) were employed. The kinetic uptake results show that the CS-50 pellet has greater sorption capacity for RB relative to FL, and this may relate to the offset in the initial dye concentration. However, a noteworthy observation is the markedly different kinetic profiles obtained for CS-50 with each respective dye. The results are in parallel agreement with the relative molecular size of each dye. Figure 6c shows that the diffusion of FL into the pellets was 4-fold greater with a steeper slope relative to RB, where the uptake of FL took about 200 min to achieve saturation of CS-50 versus ca. 800 min for the RB dye system. The observed trend for the kinetic profiles concur with the uptake results at equilibrium (*cf.* Figure 6a), where CS-50 displayed a greater uptake of FL over RB. Furthermore, to ascertain the relative magnitude of binding of FL and RB dyes onto CP materials after sorption, the samples were analyzed using DSC, as shown in Figure 6d. The T_{max} and the transition enthalpy for CP (*cf.* Figure 6d) and CS-50 after equilibrium sorption with FL and RB are shown in Table 2. There is evidence of a nearly 2-fold increase for the transition enthalpy change for CS-50 relative to CP for the FL dye system, whereas a smaller enthalpy increase of 37 J/g occurs for the RB dye system. The $\Delta_{trs}H$ parameters in Table 2 provide evidence for the higher sorption affinity of the composite pellets with FL over RB, along with important hydration contributions to the adsorption process.

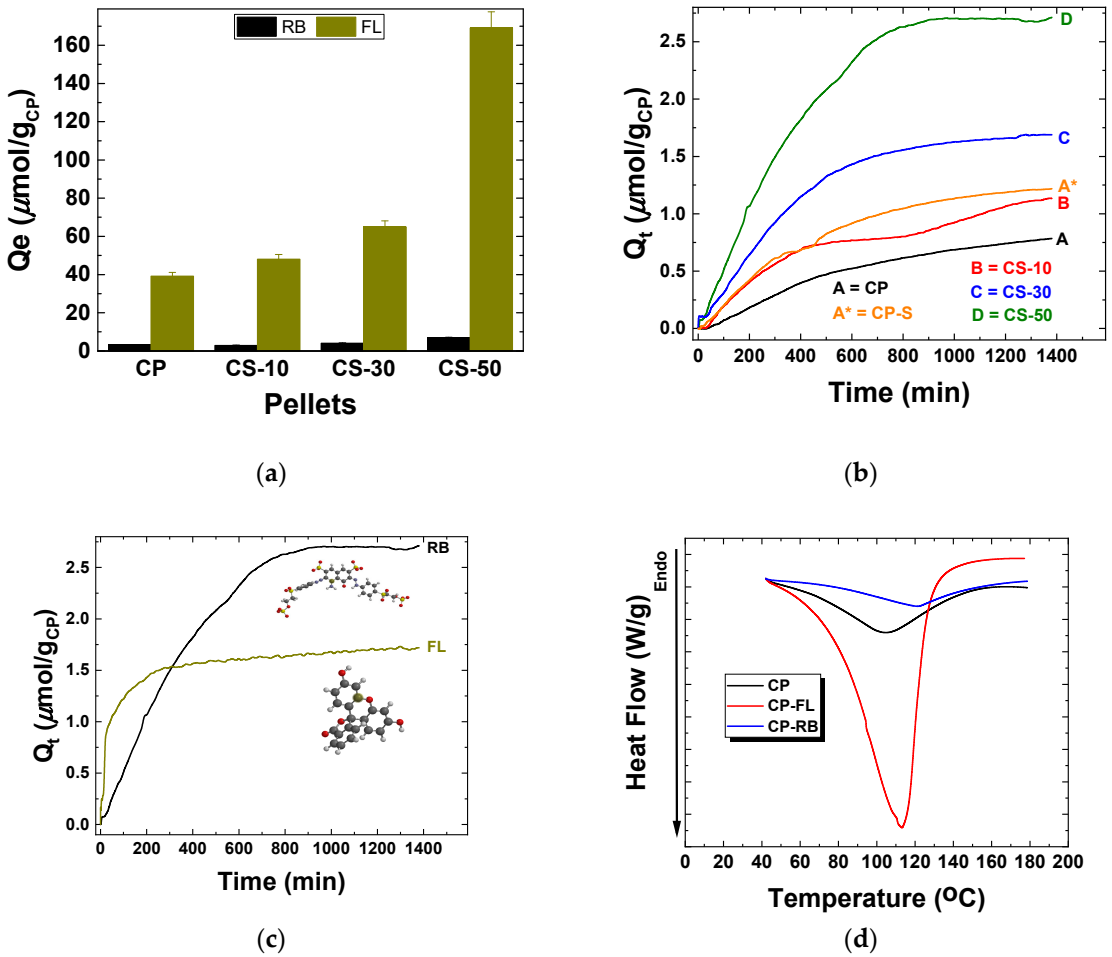

Figure 6. (**a**,**b**) Equilibrium and in situ kinetic uptake of reactive black (RB) by CP, CP-S, CS-10, CS-30, CS-50, respectively; (**c**) in situ kinetic uptake of RB and fluorescein (FL) by CS-50, and (**d**) DSC profiles for the CP system before and after adsorption of each dye.

Table 2. T_{max} values and the change in transition enthalpy ($\Delta_{trs}H$) from DSC for the single components and the composite materials.

Sample	T_{max} (°C)	$\Delta_{trs}H$ (J/g)
CP-F	113 ± 0.3	1024 ± 31
CP-R	121 ± 0.4	303 ± 9.1
CS-50-F	105 ± 0.3	1840 ± 55
CS-50-R	101 ± 0.3	340 ± 10

4. Conclusions

Composite materials (CS) that contain chitosan (C) and torrefied straw (S) were prepared as extruded pellets with variable S-content (10, 30, and 50 wt %). FT-IR/^{13}C NMR spectroscopy, TGA, and DSC provided evidence for the composition of the pelletized composite materials. The use of confocal microscopy (CLSM) with FL as the dye probe showed the presence of voids in the CS materials that increased with greater levels of S incorporation. Furthermore, the dye uptake studies using FL and RB dyes at equilibrium and kinetic conditions revealed that the composite pellets have a higher sorption affinity and kinetic uptake for FL compared to RB. The trends in the kinetics of adsorption relate to differences in the size and dipole moment of the dyes, where FL is smaller with a lower dipole moment (less tendency to partition into water in the presence of the CS pellet) relative to RB that displays improved kinetic adsorption properties. The widespread utility of chitosan adsorbent technology combined with the need to reduce material and production costs underscores the importance of this study to the field of composite science. This research illustrates the utility of blending an inexpensive biomass waste product (straw) with chitosan, a more expensive commodity biopolymer material, to yield a valorized biomaterial composite with unique physicochemical properties. The resulting composite material has improved adsorption properties with lower material cost when compared with pristine chitosan. Further studies are underway to gain insight on the sorption mechanism for uptake of adsorbates using CS composite materials across a wider range of adsorption-based applications.

Author Contributions: Conceptualization, M.H.M. and I.A.U.; Methodology, M.H.M. and I.A.U.; Software, M.H.M. and I.A.U.; Validation, M.H.M., I.A.U. and L.D.W.; Formal Analysis, M.H.M. and I.A.U.; Investigation, M..H.M., I.A.U. and L.D.W.; Resources, L.D.W.; Data Curation, M.H.M., I.A.U. and L.D.W.; Writing–Original Draft Preparation, M.H.M. and I.A.U.; Writing–Review & Editing, M.H.M., I.A.U., and L.D.W.; Supervision, L.D.W.; Project Administration, L.D.W.; Funding Acquisition, L.D.W. All authors have read and agreed to the published version of the manuscript.

Funding: The authors are grateful to the University of Saskatchewan and the support provided by the Government of Saskatchewan (Ministry of Agriculture) through the Agriculture Development Fund (Project 20170247) for this research. The APC was funded by the *Journal of Composites Science* (mdpi.com/journal/jcs) as part of a special issue invitation.

Acknowledgments: Professor Richard Evitts at the University of Saskatchewan is kindly acknowledged for providing research samples of torrefied wheat straw biomass for this research. Mostafa Solgi and Bernd Steiger are also acknowledge for helping with pellets production and straw grinding, respectively.

Conflicts of Interest: The authors declare no conflict of interest.

References

1. Tursi, A. A review on biomass: Importance, chemistry, classification, and conversion. *Biofuel Res. J.* **2019**, *6*, 962–979. [CrossRef]
2. Parmar, K. Biomass—An Overview on Composition Characteristics and Properties. *IRA-Int. J. Appl. Sci.* **2017**, *7*, 43–51. [CrossRef]
3. Passoth, V.; Sandgren, M. Biofuel production from straw hydrolysates: Current achievements and perspectives. *Appl. Microbiol. Biotechnol.* **2019**, *103*, 5105–5116. [CrossRef]
4. Zargar, V.; Asghari, M.; Dashti, A. A Review on Chitin and Chitosan Polymers: Structure, Chemistry, Solubility, Derivatives, and Applications. *ChemBioEng Rev.* **2015**, *2*, 204–226. [CrossRef]

5. Tuck, C.O.; Pérez, E.; Horváth, I.T.; Sheldon, R.A.; Poliakoff, M. Valorization of Biomass: Deriving More Value from Waste. *Science* **2012**, *337*, 695–699. [CrossRef] [PubMed]
6. Sangon, S.; Hunt, A.; Attard, T.; Mengchang, P.; Ngernyen, Y.; Supanchaiyamat, N. Valorisation of waste rice straw for the production of highly effective carbon based adsorbents for dyes removal. *J. Clean. Prod.* **2017**, *172*, 1128–1139. [CrossRef]
7. Romar-Gasalla, A.; Coelho, F.G.; Nóvoa-Muñoz, C.J.; Arias-Estévez, M.; Fernández-Sanjurjo, J.M.; Álvarez-Rodríguez, E.; Núñez-Delgado, A. Wheat Straw as a Bio-Sorbent for Arsenate, Chromate, Fluoride, and Nickel. *Water* **2017**, *9*, 690. [CrossRef]
8. Kyzas, Z.G.; Bikiaris, N.D. Recent Modifications of Chitosan for Adsorption Applications: A Critical and Systematic Review. *Mar. Drugs* **2015**, *13*, 312–337. [CrossRef]
9. Qin, C.; Li, H.; Xiao, Q.; Liu, Y.; Zhu, J.; Du, Y. Water-solubility of chitosan and its antimicrobial activity. *Carbohydr. Polym.* **2006**, *63*, 367–374. [CrossRef]
10. Pirbazari, A.E. Surfactant-Modified Wheat Straw: Preparation, Characterization and its Application for Methylene Blue Adsorption from Aqueous Solution. *J. Chem. Eng. Process Technol.* **2015**, *6*, 231. [CrossRef]
11. Mahaninia, M.H.; Wilson, L.D. Phosphate uptake studies of cross-linked chitosan bead materials. *J. Colloid Interface Sci.* **2017**, *485*, 201–212. [CrossRef] [PubMed]
12. Kim, T.-Y.; Park, S.-S.; Cho, S.-Y. Adsorption characteristics of Reactive Black 5 onto chitosan beads cross-linked with epichlorohydrin. *J. Ind. Eng. Chem.* **2012**, *18*, 1458–1464. [CrossRef]
13. Bertolino, V.; Cavallaro, G.; Milioto, S.; Parisi, F.; Lazzara, G. Thermal Properties of Multilayer Nanocomposites Based on Halloysite Nanotubes and Biopolymers. *J. Compos. Sci.* **2018**, *2*, 41. [CrossRef]
14. Bertolino, V.; Cavallaro, G.; Lazzara, G.; Milioto, S.; Parisi, F. Halloysite nanotubes sandwiched between chitosan layers: Novel bionanocomposites with multilayer structures. *New J. Chem.* **2018**, *42*, 8384–8390. [CrossRef]
15. Lisuzzo, L.; Cavallaro, G.; Parisi, F.; Milioto, S.; Fakhrullin, R.; Lazzara, G. Core/shell gel beads with embedded halloysite nanotubes for controlled drug release. *Coatings* **2019**, *9*, 70. [CrossRef]
16. You, J.; Xie, S.; Cao, J.; Ge, H.; Xu, M.; Zhang, L.; Zhou, J. Quaternized Chitosan/Poly(acrylic acid) Polyelectrolyte Complex Hydrogels with Tough, Self-Recovery, and Tunable Mechanical Properties. *Macromolecules* **2016**, *49*, 1049–1059. [CrossRef]
17. Shankar Tumuluru, J.; Sokhansanj, S.; Hess, J.R.; Wright, C.T.; Boardman, R.D. REVIEW: A review on biomass torrefaction process and product properties for energy applications. *Ind. Biotechnol.* **2011**, *7*, 384–401. [CrossRef]
18. Pereira, M.R.; Marques, J.S.; Fonseca, J.L.C. Biocomposites based on chitosan and carnauba straw powder. *Polímeros* **2014**, *24*, 446–452. [CrossRef]
19. Bai, X.; Wang, G.; Wang, D.; Wang, Z.; He, C.; Wu, H.; Liu, W. Co-pelletization of torrefied wheat straw and peanut shells. *Bioresour. Technol.* **2017**, *233*, 373–381. [CrossRef]
20. Udoetok, I.A.; Wilson, L.D.; Headley, J. V Self-Assembled and Cross-Linked Animal and Plant-Based Polysaccharides: Chitosan–Cellulose Composites and Their Anion Uptake Properties. *ACS Appl. Mater. Interfaces* **2016**, *8*, 33197–33209. [CrossRef]
21. Mohamed, M.H.; Udoetok, I.A.; Wilson, L.D.; Headley, J. V Fractionation of carboxylate anions from aqueous solution using chitosan cross-linked sorbent materials. *RSC Adv.* **2015**, *5*, 82065–82077. [CrossRef]
22. Zheng, A.; Jiang, L.; Zhao, Z.; Huang, Z.; Zhao, K.; Wei, G.; Wang, X.; He, F.; Li, H. Impact of Torrefaction on the Chemical Structure and Catalytic Fast Pyrolysis Behavior of Hemicellulose, Lignin, and Cellulose. *Energy Fuels* **2015**, *29*, 8027–8034. [CrossRef]
23. Pašalić, H.; Tunega, D.; Aquino, A.J.A.; Haberhauer, G.; Gerzabek, M.H.; Lischka, H. The stability of the acetic acid dimer in microhydrated environments and in aqueous solution. *Phys. Chem. Chem. Phys.* **2012**, *14*, 4162–4170. [CrossRef] [PubMed]
24. Murthy, N.S. 9-Techniques for analyzing biomaterial surface structure, morphology and topography. In *Woodhead Publishing Series in Biomaterials*; Williams, R., Ed.; Woodhead Publishing: Cambridge, UK, 2011; pp. 232–255. ISBN 978-1-84569-640-5.

25. Hurst, G.A.; Novakovic, K. A facile in situ morphological characterization of smart genipin-crosslinked chitosan–poly(vinyl pyrrolidone) hydrogels. *J. Mater. Res.* **2013**, *28*, 2401–2408. [CrossRef]
26. Zu, Y.; Bi, J.; Yan, H.; Wang, H.; Song, Y.; Zhu, B.-W.; Tan, M. Nanostructures Derived from Starch and Chitosan for Fluorescence Bio-Imaging. *Nanomaterials* **2016**, *6*, 130. [CrossRef] [PubMed]